Chinese Chemical Letters 34 (2023) 107828

Contents lists available at ScienceDirect

Chinese Chemical Letters

journal homepage: www.elsevier.com/locate/cclet

Cell membrane-coated mesoporous silica nanorods overcome sequential drug delivery barriers against colorectal cancer

Jie Wang[a,b,c,1], Hao Pan[d,1], Jingyi Li[a], Di Nie[a,e], Yan Zhuo[a], Yishan Lv[a,b], Ning Wang[a,e], Hao Chen[e,f], Shiyan Guo[a,e], Yong Gan[a,e], Xinggang Yang[b,*], Miaorong Yu[a,e,**]

[a] State Key Laboratory of Drug Research, Shanghai Institute of Materia Medica, Chinese Academy of Sciences, Shanghai 201203, China
[b] School of Pharmacy, Shenyang Pharmaceutical University, Shenyang 110016, China
[c] School of Pharmacy, Shanghai University of Traditional Chinese Medicine, Shanghai 201203, China
[d] College of Pharmacy, Liaoning University, Shenyang 110036, China
[e] University of Chinese Academy of Sciences, Beijing 100049, China
[f] Molecular Imaging Center, Shanghai Institute of Materia Medica, Chinese Academy of Sciences, Shanghai 201203, China

ARTICLE INFO

Article history:
Received 29 June 2022
Revised 9 September 2022
Accepted 14 September 2022
Available online 17 September 2022

Keywords:
Cell membrane coating
Rod shape
Sequential delivery
Nuclear accumulation
Colorectal cancer

ABSTRACT

Local delivery of nanomedicines holds therapeutic promise for colorectal cancer (CRC). However, it presents tremendous challenges due to the existence of multiple physiological barriers, especially intracellular obstacles, including intracellular trafficking, subcellular accumulation, and drug release. Herein, we report a multifunctional nanoparticle (CMSNR) by wrapping the mesoporous silica nanorod with cell membrane derived from CRC cells for improved chemotherapy. Compared with their naked counterparts, the cell membrane endowed CMSNR with homotypic targeting and improved cellular uptake capacities. Due to the rod-like shape, CMSNR achieved superior colorectal mucus permeability, enhanced tumor accumulation, and boosted cellular uptake than their spherical counterparts. Moreover, the internalized CMSNR underwent robust intracellular trafficking and gained augmented motility toward the nucleus, leading to efficient perinuclear accumulation and a subsequent 5.6-fold higher nuclear accumulation of loaded drug than that of nanospheres. In the orthotopic colorectal tumor-bearing nude mice, rectally administrated mefuparib hydrochloride (MPH)-loaded CMSNR traversed the colorectal mucus, penetrated the tumor tissue, and successfully aggregated in the perinuclear region of cancer cells, thus exhibiting significantly improved antitumor outcomes. Our findings highlight the shape-based design of cell membrane-coated nanoparticles that can address sequential drug delivery barriers has a promising future in cancer nanomedicine.

Colorectal cancer (CRC) is the third most prevalent cancer and the second leading cause of cancer-related death worldwide [1]. Almost half of the CRC patients are diagnosed at late-stages, for which chemotherapy is often the primary treatment [2]. However, low drug accumulation in the tumor tissue *via* systemic administration always results in compromised outcomes. Currently, researches have shown that local delivery of nanomedicines for CRC could possess advantages of high efficacy and low side effects but also presents tremendous challenges [3]. The sequential drug delivery barriers, including mucus, tumor penetration and accumulation, cellular uptake, and intracellular drug release [4–7], would significantly impair the delivery efficacy of nanomedicine. Decorating the nanoparticles with dense polyethylene glycol (PEG) can boost their mucus diffusivity and enhance tumor permeability [8,9]. The cellular internalization of nanoparticles can be ameliorated by surface modification of targeting ligands (*e.g.*, folic acid [10]). Nevertheless, restricted intracellular transport and inefficient subcellular drug accumulation remain the major obstacles to address. As the most frequent targets of chemotherapeutics (*e.g.*, 5-fluorouracil [11,12]) are usually located in the nucleus, nanoparticles, which could effectively deliver the loaded drugs into the nucleus, may fully realize the therapeutic potential. Recent studies have revealed that the amount of drug in the nucleus is usually much lower than the internalized amount [13–15], suggesting that challenges still persist. Therefore, nanoparticles capable of over-

* Corresponding author.
** Corresponding author at: State Key Laboratory of Drug Research, Shanghai Institute of Materia Medica, Chinese Academy of Sciences, Shanghai 201203, China.
E-mail addresses: yangxg123@163.com (X. Yang), mryu@simm.ac.cn (M. Yu).
[1] These authors contributed equally to this work.

https://doi.org/10.1016/j.cclet.2022.107828
1001-8417/

coming the multiple obstacles step by step, especially the intracellular trafficking barriers, are urgently needed.

Inspired by the shape of pathogens [16,17], nanoparticles with various shapes have been designed, and they exhibited superiorities in facilitating many aspects of the drug delivery processes [18–20]. For example, rod-like nanoparticles are reported to address one or several physical obstacles [21,22], such as superior mucus diffusivity [23], improved tumor accumulation [24], enhanced cellular uptake [25], and facilitated intracellular trafficking [26], thus providing a strong indication on the design of rod-like nanoparticles to overcome multiple drug delivery barriers for CRC treatment sequentially. However, due to the difficulty in fabrication, the majority of rod-like nanoparticles are inorganic, which might lead to compromised cellular uptake and further limited subcellular accumulation. Recently, Zhang *et al*. [27], have pioneered in developing cell membrane-coated nanoparticles for effective drug delivery. By camouflaging nanomaterials with a layer of the natural cell membrane, the obtained nanoparticles not only preserve the functionalities of the inner core particle but also acquire the unique characteristics associated with cell membranes, such as high biocompatibility, homing targeting, and enhanced cellular uptake [28,29]. Therefore, we hypothesize that nanorods cloaked in a layer of cell membrane-derived from CRC cells might accelerate nanoparticle internalization and intracellular transportation, thus successfully conquering the sequential drug delivery barriers.

Herein, we reported the design of cancer cell membrane (CCM)-coated mesoporous silica nanorods (CMSNR) to overcome sequential drug delivery barriers for enhanced chemotherapy against CRC. We showed that CMSNR successfully conquered the colorectal mucus, efficiently penetrated the tumor tissue, easily entered cancer cells, and underwent facilitated intracellular trafficking, resulting in remarkable aggregation around the nucleus as well as sufficient delivery of the loaded drug into the nucleus. In an orthotopic CRC nude mouse model, rectally administrated CMSNR loaded with mefuparib hydrochloride (MPH) achieved better tumor suppression than their spherical counterparts. Our findings highlight the shape design of cell membrane-coated nanoparticles, and CMSNR stands as a promising approach to overcoming sequential drug delivery barriers for cancer chemotherapy.

To construct CMSNR, rod-shaped mesoporous silica nanoparticles (MSNR) were first fabricated as cores following the literature procedure [30,31]. Cell membranes derived from human colorectal cancer (HT-29) cells were then extracted by gradient density centrifugation to obtain CCM vesicles, followed by the fusion with MSNR *via* ultrasonication to generate the core-shell-structured CMSNR (Fig. 1A). Besides, we prepared cell membrane-coated mesoporous silica nanospheres (CMSNS) and naked nanospheres (MSNS) and nanorods (MSNR) as controls.

The average hydrodynamic diameters of CMSNR and CMSNS were approximately 110 nm, while MSNR and MSNS were approximately 100 nm. The surface charge of the CMSNR (-22.5 ± 1.0 mV) and CMSNS (-22.7 ± 1.4 mV) was close to that of CCM (-22.2 ± 0.7 mV), confirming that CMSNR and CMSNS were successfully coated with CCM (Figs. 1B and C and Table S1 in Supporting information). The morphology of nanoparticles was visualized *via* transmission electron microscope (TEM), showing highly monodispersed spherical MSNS and rod-like MSNR and their corresponding core-shell structured CMSNS and CMSNR (Fig. 1D and Fig. S1 in Supporting information). The MSNR and CMSNR had a dimension of approximately 50 nm × 150 nm, and 65 nm × 165 nm, respectively. Meanwhile, confocal laser scanning microscopy (CLSM) and stimulated emission depletion (STED) microscopy imaging confirmed the core-shell structure of CMSNR and CMSNS (Fig. 1E), which was consistent with the results of fluorescence resonance energy transfer (FRET) analysis, where the emission intensity of FITC-MSNs declined at 520 nm, and the paired fluorophore was increased at the corresponding wavelength (Fig. S2 in Supporting information).

The protein compositions of CMSNS and CMSNR were similar to those of CCM vesicles measured by sodium dodecyl sulfate-polyacrylamide gel electrophoresis (SDS-PAGE) analysis (Fig. 1F). And CD151, one of the surface adhesion molecules on the HT-29 cells [32], was also confirmed to transferred to the shell of CMSNR and CMSNS by western blotting analysis, indicating that the cancer cell membrane proteins were retained (Fig. 1G).

MPH, a poly(ADP-ribose) polymerase (PARP)1/2 inhibitor [33], was used as the model drug. The loading capacity (LC%) and encapsulation efficiency (EE%) for all the nanoparticles were approximately 15% and 45%, respectively (Table S1). The *in vitro* MPH release profile in PBS (pH 7.4 and 6.0) demonstrated that the coating of CCM notably delayed MPH release from MSNR and MSNS. Approximately 65% of MPH was released from CMSNS and CMSNR within 24 h, while over 80% of MPH was released from MSNR and MSNS (Fig. S3 in Supporting information).

In addition, the obtained nanoparticles displayed good colloidal and fluorescent stability, and they also showed no obvious cytotoxicity within the tested concentrations (Figs. S4–S6 in Supporting information). Collectively, we successfully fabricated the cancer cell membrane-coated nanorods with good stability and biocompatibility.

We then investigated whether CMSNR could improve mucus diffusion capacity by using multiple-particle tracking (MPT) technology [34]. The PEGylated MSNS (PMs), a kind of mucus penetrating particles (Table S1), were fabricated as the positive control. The total particle motion in the mucus was calculated by aggregating the results of 200 particles. It showed that the rod-like nanoparticles obtained broader movement areas than the corresponding spherical counterparts, and CMSNR exhibited the largest diffusion areas (Fig. 2A). The time-mean square displacement (MSD) value at 1 s of CMSNR was approximately 6.0-fold and 24.6-fold higher than that of CMSNS and MSNS (Fig. 2B), respectively. The effective diffusivity (D_{eff}) of nanoparticles also showed the superior mucus diffusion capacities of CMSNR (Fig. 2C). These results suggested that the CMSNR could penetrate the mucus efficiently.

The penetration ability of nanoparticles in multicellular spheroids (MCSs) was then quantitatively and qualitatively monitored by CLSM (Figs. 2D and E). It showed that CMSNR displayed superior penetration at all scanning depths compared with other nanoparticles, and more CMSNR accumulated in the MCSs, showing a 4.9-fold higher fluorescence intensity than that of the MSNS group at the scanning depth of 100 μm.

We next explored whether the cell membrane-coated nanoparticles could have self-recognition ability of the corresponding homologous cell line with enhanced cellular internalization. The results revealed that CMSNR, CMSNS and CCM were internalized more efficiently by HT-29 cells than Huh-7, Bxpc-3, Hela, MCF-7 cells (Fig. S7 in Supporting information), and CMSNR and CMSNS displayed improved cellular uptake than the uncapped nanoparticles (Figs. 2F and G), indicating the selected targeting of homotypic tumor cells. In addition, the MSN core and cell membrane shell were labeled with FITC and DiI, respectively. The CLSM images demonstrated that the green fluorescence derived from MSNS and MSNR perfectly matched well with the red fluorescence derived from the outer shell (Fig. 2H), indicating the intracellular integrity of CCM-coated nanoparticles.

To further investigate the endocytosis mechanisms of CMSNR, we utilized three different endocytosis inhibitors (chlorpromazine, CPZ) for the inhibition of clathrin-mediated endocytosis, filipin (FLP) for the inhibition of caveolae-mediated endocytosis, and dynasore (DNS) for the inhibition of both clathrin- and caveolin-mediated endocytosis). The results were consistent with those pre-

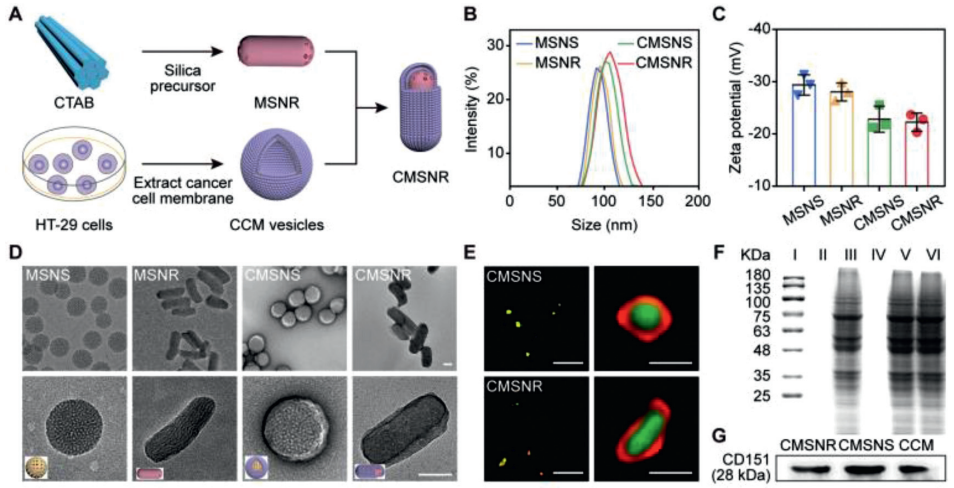

Fig. 1. Preparation and characterization of nanoparticles. (A) Fabrication of CMSNR nanoparticles. (B) The size and (C) zeta potential of various nanoparticles ($n = 3$). (D) TEM images of CMSNR, CMSNS, MSNR, MSNS. Scale bar: 50 nm. (E) Confocal images (left) and super-resolution images (right) of CCM-coated nanoparticles. Red: DiI-labeled CCM; green: FITC-labeled MSNS or MSNR. Scale bar: 500 nm (left) and 100 nm (right). (F) SDS-PAGE analysis of marker, MSNS, CMSNS, MSNR, CMSNR and CCM vehicles (I-VI). Samples were prepared with equal amounts of protein, followed by staining with Coomassie blue. (G) Western blot analysis of the expression of CD151 on the membrane isolated from the indicated nanoparticles was developed.

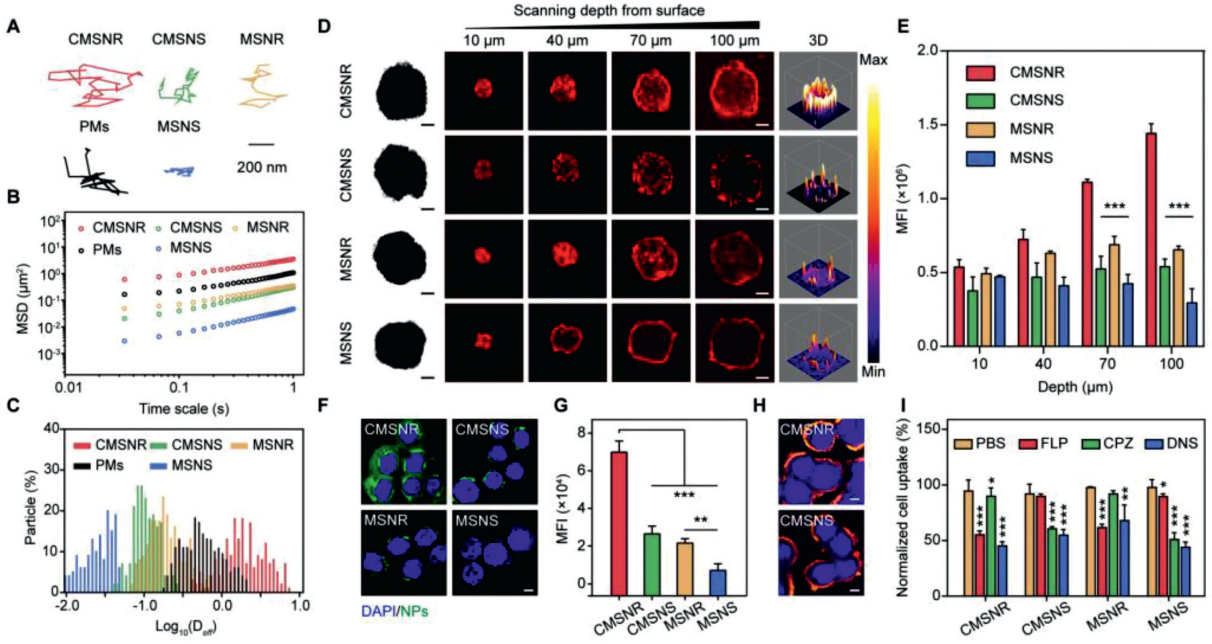

Fig. 2. MCS penetration and cellular internalization of nanoparticles. (A) Representative trajectories for particles in the colorectal mucus on a time scale of 1 s. (B) Ensemble-averaged geometric MSD values of nanoparticles as a function of time scale. (C) Distributions of the logarithms of individual particle effective diffusivities at a time scale of 1 s ($n = 200$). (D) *In vitro* penetration of RITC-labeled nanoparticles (red) in HT-29 MCSs. MCSs were incubated with different nanoparticles and imaged by CLSM z-stack scanning after 4 h. The MCS surface was settled at 0 μm. Scale bar: 100 μm. (E) Quantification analysis of particle penetration in HT-29 MCSs. $^{***}P < 0.001$. (F) CLSM images of the endocytosis of nanocarriers in HT-29 cell lines. Blue: nuclei stained with DAPI. Green: FITC-labeled nanoparticles. Scale bar: 10 μm. (G) Quantitative determination of the cellular uptake amounts of nanoparticles in HT-29 cells. $^{**}P < 0.01$, $^{***}P < 0.001$. (H) Intracellular co-localization of the CCM shell (red) and the MSNR and MSNS core (green). Blue: nuclei stained with DAPI. Scale bar: 10 μm. (I) Quantification of nanoparticles internalized in HT-29 cells pretreated with CPZ, FLP and DNS. $^{*}P < 0.05$, $^{**}P < 0.01$, $^{***}P < 0.001$.

viously reported [35–37] that the rod-like nanoparticles could be taken up *via* the caveolar pathway (Fig. 2I).

Following cellular uptake, nanoparticles still need to undergo intracellular traffic, which hinders the transport of nanoparticles toward nucleus. To explore the intracellular transport capacities of CMSNR, we incubated HT-29 cells with FITC-labeled nanoparticles for 2 h and tracked their intracellular movement by CLSM (Fig. S8 in Supporting information). Upon internalization, CMSNR diffused freely within the cytoplasm and ultimately reached the perinuclear region, while CMSNS diffused only into the peripheral area of the cytoplasm. Furthermore, we examined the dynamics of particle transport in HT-29 cells using fluorescent imaging and a two-dimensional single-particle tracking technique. Representative trajectories showed that the majority of nanospheres were confined in a small area, while CMSNR moved rapidly toward the perinuclear region (Fig. 3A). Quantitative analysis of particle movement showed that the average speed of CMSNR was 0.174 μm/s, which was 1.1-, 1.9- and 2.4-fold higher than that of MSNR (0.155 μm/s), CMSNS (0.094 μm/s) and MSNS (0.072 μm/s), respectively (Fig. 3B). In addition, the corresponding colorimetric distribution maps of

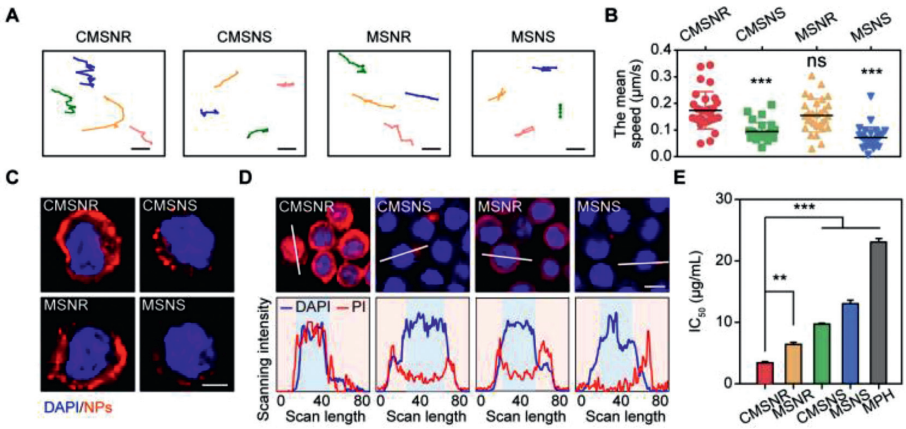

Fig. 3. Dynamics of intracellular transport, perinuclear aggregation, and cell viability of nanoparticles. (A) Representative trajectories of different nanoparticles. Scale bar: 4 μm. (B) The mean speed of intracellular transport of nanoparticles. $^{***}P < 0.001$, ns represented no significant difference. (C) CLSM images of nanoparticles distributions in HT-29 cells; red, nanoparticles. Scale bar: 10 μm. (D) CLSM images and line-scan profiles of fluorescence intensity for HT-29 cells incubated for 4 h with PI-loaded nanoparticles. Red: PI. Blue: cell nuclei stained with DAPI. The concentration of PI is 1 μg/mL ($n = 3$). Scale bar: 20 μm. (E) Cell viability of MPH-loaded nanoparticles in HT-29 cells measured by the CCK-8 kit. $^{**}P < 0.01$, and $^{***}P < 0.001$.

CMSNR within the cells also showed that the CMSNR agglomerated in the perinuclear region in HT-29 cells (Fig. 3C and Fig. S9 in Supporting information). The colocalization studies showed that the internalized CMSNS and MSNS were mostly located in the late endosome and lysosomal compartments and CMSNR and MSNR could bypass lysosome entrapment (Fig. S10 in Supporting information). These results consistently showed that the CMSNR exhibited robust intracellular trafficking toward nucleus with higher motility than their spherical counterparts.

To explore whether the perinuclear accumulation of nanoparticles could benefit nuclear drug delivery, propidium iodide (PI), a commonly used water-soluble fluorescent dye which cannot diffuse into the nucleus, was loaded in the CMSNR. The distribution of PI in the cells were mapped. As depicted in Fig. 3D and Fig. S11 (Supporting information), free PI signals were not observed in living cells. A low amount of PI was detected in the nuclei of the cells treated with CMSNS and MSNS. However, PI loaded in CMSNR was distributed throughout the entire cell, including the nucleus. The efficacy of PI dye entry into the nucleus was approximately 66.23% for CMSNR, which was 4.8-, 2.0- and 9.5-fold higher than that for CMSNS, MSNR, and MSNS, respectively (Fig. S12 in Supporting information). Additionally, a CCK-8 Kit assay was performed to analyze the *in vitro* cytotoxicity of MPH-loaded nanoparticles. The CMSNR displayed the lowest half-maximal inhibitory concentration (IC_{50}) value of 3.4 μg/mL among all the samples (Fig. 3E). Therefore, CMSNR, which could be transported close to the nucleus, delivered significantly more MPH into the nucleus, resulting in enhanced cytotoxicity.

To represent the delivery efficacy of CMSNR *in vivo*, we established an orthotopic colorectal cancer model using HT-29 cells according to previous literature [38]. After dissection, the tumor tissue can be found by the naked eye compared with the non-tumor area (Fig. S13 in Supporting information, black arrows). The normal colon wall is smooth and intact, but the colon wall, after injection of the HT-29 cells, has a prominent tumor mass. The hematoxylin and eosin (H&E) staining study further confirmed that we have successfully constructed the orthotopic HT29 colorectal tumor model.

Based on *in vitro* diffusion results, CMSNR is supposed to penetrate colon mucus efficiently. We next explored particle mucus penetration in the colorectal loops of tumor-bearing mice. The results showed that CMSNS and MSNS could not effectively penetrate the mucus, and only a few particles were detected in the upper layer. In contrast, CMSNR were transported deeper along the z-direction, suggesting that CMSNR maintained their superiority in mucus penetration *ex vivo* (Fig. S14 in Supporting information).

We then evaluated the tumor accumulation of nanocarriers *in vivo*. Nanoparticles were labeled with CH1055, a second near-infrared window (NIR-II) fluorophore, and then rectally administrated into HT-29 tumor-bearing nude mice. The fluorescence intensity of these four nanoparticles in the tumor sites decreased over time (Figs. 4A and B). The fluorescence intensity of MSNS, MSNR, and CMSNS decreased quickly, but that of CMSNR decreased gradually, which might be resulted from their facilitated colorectal mucus diffusion, homologous targeting, and enhanced internalization capabilities.

Relying on the HT-29 cell membrane coating, CMSNR possessed homologous active targeting, which acquired 2.6-, 4.4- and 6.2-fold tumor accumulation compared with CMSNS, MSNR and MSNS after 6 h administration (Fig. S15 in Supporting information). These results demonstrated that CMSNR could efficiently penetrate the colon mucus and tumor tissue, contributing to superior tumor accumulation.

Good mucus penetration and tumor accumulation are far from enough, and cell uptake is another crucial factor in efficiency delivery. Nanoparticles labeled with RITC dye were administrated into the mice through the rectum, and the colon tissue was sliced and examined by CLSM. In the white-outlined region, extensive areas with strong fluorescence intensities from CMSNR were detected in the perinuclear region of tumor cells, in sharp contrast to the other nanoparticles that showed limited fluorescence intensity (Fig. 4C). The quantitative analysis further revealed that the mean fluorescent intensity of CMSNR was 2.7-, 4.4- and 7.2-fold higher than that of MSNR, CMSNS and MSNS, respectively, supporting that CMSNR had the more robust tumor penetration efficiency (Fig. S16 in Supporting information).

Finally, we evaluated the *in vivo* antitumor activity against CRC of MPH-loaded nanoparticles. The mice were randomly divided into six groups and rectally administrated with various formulations every 2 d with eight repetitions (day 1, 3, 5, 7, 9, 11, 13, 15, 17, 19, 21). Limited changes in body weight were observed in all groups, indicating no overt toxicity (Fig. S17 in Supporting information). The tumors were photographed and weighed at the end of the treatment (Figs. 4D and E). The CMSNS group displayed slightly better antitumor efficiency than the MSNS group, which could be explained by the superior homology identification properties of CCM. The strongest antitumor efficiency of the CMSNR group was observed mainly due to its homologous targeting, im-

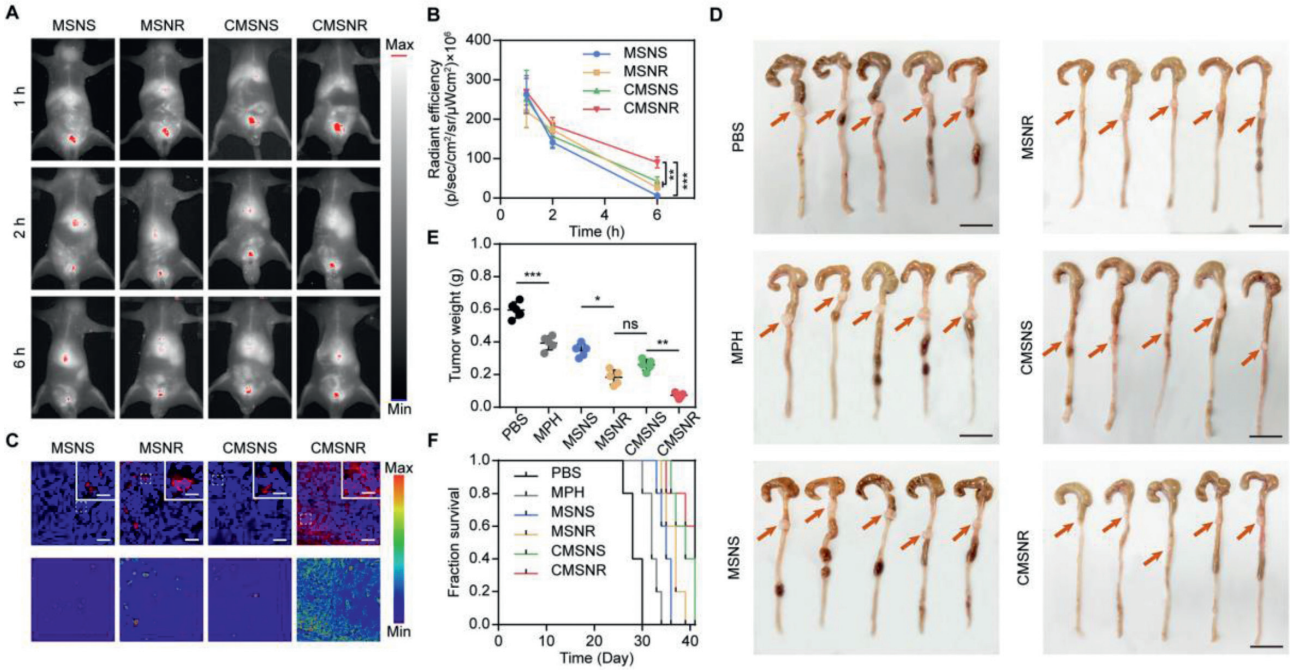

Fig. 4. The targeting and penetration capacity and *in vivo* tumor growth inhibition studies in an orthotopic CRC nude mouse model. (A) Representative *in vivo* NIR fluorescent images of HT-29 tumor-bearing mice rectally administrated with different nanoparticles labeled with CH1055. (B) Mean fluorescence intensity of nanoparticles in tumor sites at the different time points after rectally administrated. (C) CLSM images (up) and corresponding colorimetric maps (bottom) of nanoparticle distributions in the colorectal tumor sections. Scale bar: 50 μm and 15 μm (inner). (D) Photos of the tumors harvested at the end of pharmacological studies. The mice bearing HT-29 tumors were treated with the indicated formulations for 21 days. Scale bar: 1 cm. (E) Weights of tumors. $^{*}P < 0.05$, $^{**}P < 0.01$, and $^{***}P < 0.001$, ns represented no significant difference. (F) The survival time of orthotopic CRC animals following different treatments (Median survival: PBS = 28 days, MPH = 32 days, MSNS = 35 days, MSNR = 37 days, and CMSNS = 39 days). $n = 5$, $^{***}P < 0.001$.

proved mucus penetration and efficient subcellular drug delivery abilities. In addition, CMSNR prolonged the median survival time of colorectal tumor-bearing mice compared to the other groups (Fig. 4F). Although CMSNS could obtain targeting capability and enhanced internalization due to the cell membrane coating, they exhibited comparable anti-tumor outcomes with the naked MSNR, which might be resulted from their decreased mucus permeation and weakened tumor penetration.

The H&E staining of tumors revealed evident DNA damage and membrane lysis in the CMSNR group (Fig. S18 in Supporting information). This result implied that MPH-loaded CMSNR led to significant apoptosis of the tumor cells. And the degree of apoptosis decreased in the range of MSNR, CMSNS, MSNS, MPH and PBS groups. Therefore, the superiority of CMSNR in overcoming the sequential drug delivery barriers can improve the therapeutic efficacy in orthotopic CRC mice models.

In summary, we herein developed a multifunctional nanoparticle system of cell membrane-coated mesoporous silica nanorods that possess several distinct advantages in negotiating the sequential drug delivery barriers for improved cancer therapy. Compared to the typical sphere-shaped nanoparticles, CMSNR, attributed to its rod shape, exhibited facilitated colorectal mucus and tumor penetration. Owing to its CCM coating, CMSNR showed a homologous tumor-targeting ability. More importantly, after cellular uptake, CMSNR exhibited accelerated intracellular trafficking, excellent aggregation around the nucleus, and improved drug delivery efficiency into the nucleus. Consequently, an improved tumor suppression effect was achieved in orthotopic CRC nude mice models after rectally administrated MPH-loaded CMSNR. These results highlight the shape-based design of nanotherapeutics for overcoming the sequential drug delivery barriers. Given the high potency observed in the present study, this nanosystem has great potential for efficacy testing in other tumors that are highly attractive.

Declaration of competing interest

The authors report no declarations of interest.

Acknowledgments

The authors would sincerely appreciate the financial support from the National Natural Science Foundation of China (Nos. 82073773, 82104078) and the Major International Joint Research Project of Chinese Academy of Sciences (No. 153631KYSB20190020). We acknowledge the use of 120 kV TEM and CLSM-Leica SP8 at the National Center for Protein Science Shanghai. We are also very grateful to Lihui Xin, Jialin Duan and Fengming Liu for their support in the data processing and image rendering. All the animal experiments were carried out according to the Institutional Animal Care and Use Committee (IACUC) guidelines of the Shanghai Institute of Materia Medica (IACUC code: 2019–12-GY-55).

Supplementary materials

Supplementary material associated with this article can be found, in the online version, at doi:10.1016/j.cclet.2022.107828.

References

[1] H. Sung, J. Ferlay, R.L. Siegel, et al., CA Cancer J. Clin. 71 (2021) 209–249.
[2] R.M. McQuade, V. Stojanovska, J.C. Bornstein, K. Nurgali, Curr. Med. Chem. 24 (2017) 1537–1557.
[3] X. Ye, H. Yin, Y. Lu, H. Zhang, H. Wang, Molecules 21 (2016) 1347.
[4] Q. Zhou, C. Dong, W. Fan, et al., Biomaterials 240 (2020) 119902.
[5] T. Wang, D. Wang, J. Liu, et al., Nano Lett. 17 (2017) 5429–5436.
[6] E. Blanco, H. Shen, M. Ferrari, Nat. Biotechnol. 33 (2015) 941–951.
[7] Y. Zhang, T. Li, Y. Hu, et al., Chin. Chem. Lett. 33 (2022) 2507–2511.
[8] J.T. Huckaby, S.K. Lai, Adv. Drug Deliv. Rev. 124 (2018) 125–139.
[9] H. Hatakeyama, H. Akita, H. Harashima, Biol. Pharm. Bull. 36 (2013) 892–899.

[10] B. Yameen, W.I. Choi, C. Vilos, et al., J. Control. Release 190 (2014) 485–499.
[11] K. Van der Jeught, H.C. Xu, Y.J. Li, X.B. Lu, G. Ji, World J. Gastroenterol. 24 (2018) 3834–3848.
[12] X. Zhang, H. Song, B.S.B. Canup, B. Xiao, Expert Opin. Drug Deliv. 17 (2020) 781–790.
[13] X. Fu, Y. Shi, T. Qi, et al., Signal Transduct. Target Ther. 5 (2020) 262.
[14] J. Zhong, L. Li, X. Zhu, et al., Biomaterials 65 (2015) 43–55.
[15] Z. Zhou, Y. Shen, J. Tang, et al., Adv. Funct. Mater. 19 (2009) 3580–3589.
[16] L.K. Sycuro, Z. Pincus, K.D. Gutierrez, et al., Cell 141 (2010) 822–833.
[17] F. Backhed, R.E. Ley, J.L. Sonnenburg, D.A. Peterson, J.I. Gordon, Science 307 (2005) 1915–1920.
[18] V.T. Cong, K. Gaus, R.D. Tilley, J.J. Gooding, Expert Opin. Drug Deliv. 15 (2018) 881–892.
[19] J.A. Champion, Y.K. Katare, S. Mitragotri, J. Control. Release 121 (2007) 3–9.
[20] Z. Wang, Z. Wu, J. Liu, W. Zhang, Expert Opin. Drug Deliv. 15 (2018) 379–395.
[21] B.J. Lee, Y. Cheema, S. Bader, G.A. Duncan, JCIS Open 4 (2021) 100025.
[22] M. Guo, M. Wei, W. Li, et al., J. Control. Release 307 (2019) 64–75.
[23] M. Yu, J. Wang, Y. Yang, et al., Nano Lett. 16 (2016) 7176–7182.
[24] L. Zhang, H. Su, H. Wang, et al., Theranostics 9 (2019) 1893–1908.
[25] C. Bao, B. Liu, B. Li, et al., Nano Lett. 20 (2020) 1352–1361.
[26] E. Hinde, K. Thammasiraphop, H.T. Duong, et al., Nat. Nanotechnol. 12 (2017) 81–89.
[27] R.H. Fang, C.M. Hu, B.T. Luk, et al., Nano Lett. 14 (2014) 2181–2188.
[28] Z. Chen, P. Zhao, Z. Luo, et al., ACS Nano 10 (2016) 10049–10057.
[29] X. Liu, X. Zhong, C. Li, Chin. Chem. Lett. 32 (2021) 2347–2358.
[30] D.E. Owens 3rd, N.A. Peppas, Int. J. Pharm. 307 (2006) 93–102.
[31] T. Zhang, Z. Lu, J. Wang, et al., Chin. Chem. Lett. 32 (2021) 1755–1758.
[32] C.W. Chien, S.C. Lin, Y.Y. Lai, et al., Clin. Cancer Res. 14 (2008) 8043–8051.
[33] J.X. He, M. Wang, X.J. Huan, et al., Oncotarget 8 (2017) 4156–4168.
[34] M.E. Johansson, J.M. Larsson, G.C. Hansson, Proc. Natl. Acad. Sci. U. S. A. 108 (Suppl. 1) (2011) 4659–4665.
[35] X. Du, Y. Hou, J. Huang, et al., Acta Pharm. Sin. B 11 (2021) 3272–3285.
[36] J. Zhuang, D. Wang, D. Li, et al., Chin. Chem. Lett. 29 (2018) 1815–1818.
[37] C. Teng, B. Li, C. Lin, et al., J. Control. Release 341 (2022) 591–604.
[38] X. Zhu, Y. Gong, Y. Liu, et al., Biomaterials 242 (2020) 119923.